POLITECNICO DI TORINO
Repository ISTITUZIONALE

Ultra-fast photocatalytic degradation of Rhodamine B exploiting oleate-stabilized zinc oxide nanoparticles

(Article begins on next page)

12 September 2024

Discover Nano

Ultra-fast photocatalytic degradation of Rhodamine B exploiting oleate-stabilized zinc oxide nanoparticles

Nicolò Maria Percivalle[1] · Marco Carofiglio[1] · Simelys Hernández[1] · Valentina Cauda[1]

Abstract

Rhodamine B (RhB) is a harmful dye released by industrial wastewaters, thus necessitating its urgent removal. Advanced oxidation processes constitute promising strategies to purify polluted water. Among others, photocatalysis relies on reactive oxygen species (ROS) produced by photocatalytic particles, typically semiconductors like titania or zinc oxide (ZnO), excited by solar or UV–Vis light. However, their wide band gap limits their catalytic capabilities within the absorption of the UV spectrum and causes fast electron–hole recombination. This study presents novel strategies to overcome these limitations: (i) doping semiconductors to increase photocatalytic efficiency; (ii) sensitization-mediated photocatalysis for visible light activation using chemical moieties to trap dye molecules; (iii) nanosizing the photocatalysts to enhance the surface area. ZnO nanoparticles, doped with iron or gadolinium and capped with oleic acid are here synthesized and tested in RhB dye solutions. Remarkably, the results demonstrate an ultra-fast RhB degradation, driven by oleic acid having crucial role in dye adsorption. The degradation mechanisms, including ROS-induced N-deethylation and xanthene group cleavage, are also unraveled. These findings underscore the efficacy of the proposed semiconductor photocatalyst design, highlighting a significant advancement with extensive potential applications in wastewater remediation. This innovative approach paves the way for more efficient and practical solutions to combat industrial dye pollution.

Keywords Zinc oxide · Capping agent · Doping · Photodegradation · ROS

1 Introduction

Environmental pollution and contextually water pollution are prominent concerns, counterbalancing the positive aspects brought by industrialization, and gaining high recognition over time [1–3]. Textile industries are one of the main responsible contributing to water pollution, particularly due to the discharge of effluents from factories. These industrial effluents contain several polluting agents, among which dyes constitute the main contaminant of wastewater [4, 5]. Rhodamine B (RhB), among other dyes, is attracting particular interest in recent years because of its harmful nature. It is a persistent organic pollutant (POP) that is resistant to environment degradation and have been continuously released into the environment. It causes increasing concerns due to its mutagenic and cancerogenic characteristics that make it extremely dangerous for human beings and wildlife. Furthermore, it affects the photosynthesis and the natural purification processes of

✉ Simelys Hernández, simelys.hernandez@polito.it; ✉ Valentina Cauda, valentina.cauda@polito.it | [1]Department of Applied Science and Technology, Politecnico Di Torino, Corso Duca Degli Abruzzi 24, 10129 Turin, Italy.

aquatic plants by preventing light penetration [6]. Based on these considerations, RhB removal from wastewater seems inevitable to preserve the well-being and the balance of the ecosystem. Nowadays, the wastewater reclamation and reuse are of prominent importance in view of the increasing water scarcity and poor water resource management [7].

Advanced oxidation processes (AOPs) represent a group of chemical oxidating methods and have been proposed in the last decade as an effective way of purifying polluted wastewaters. They enable to overcome the major disadvantages related to the conventional treatment methods, namely low removal efficiency, long purification times and post-treatments, while allowing for a fast degradation rate, the complete mineralization of organic compounds, or their conversion to green products. Furthermore, AOP can operate under ambient temperature and pressure [8]. AOPs can be categorized in Fenton oxidation (Fe^{2+}/H_2O_2), Fenton-like oxidation (Fe^{3+}/H_2O_2), photo-assisted Fenton ($Fe^{2+/3+}/H_2O_2/UV$); photocatalysis ($TiO_2/hv/O_2$), ozone systems (O_3/H_2O_2, O_3/UV), UV photolysis (UV/H_2O_2), as well as sonolysis and sonocatalysis [9]. While the diverse AOPs are characterized by different mechanisms of action, their common outcome is the generation of reactive oxygen species (ROS), notably hydroxyl radicals $\cdot OH$, superoxide anion $\cdot O_2^-$, and singlet oxygen $^1O_2$, which are able to act as oxidizing agents to drive dyes decomposition.

Among several AOPs, photocatalysis has attracted interest over the past few years as a purification method for polluted wastewater due to its non-selective oxidation capabilities, procedural simplicity, and cost effectiveness [10, 11]. This reaction relies on the presence of a light-absorbing catalyst which, upon light irradiation, triggers the dye degradation with whom it is in contact. Two different photodegradation mechanisms are distinguishable: the direct photodegradation process and the sensitization-mediated one. The first one exploits the photoexcitation of a semiconductor catalyst which promotes the shifting of an excited electron from the valence band (VB) to the conduction band (CB); the generated electron–hole pair can react with the surrounding molecules leading to the production of the abovementioned reactive oxygen species. ROS can then oxidize or degrade the dye molecules adsorbed on the catalyst surface. On the other hand, the sensitization-mediated process exploits the capabilities of the adsorbed dye to be excited under visible light irradiation, thus producing photoexcited electron at its lowest unoccupied molecular orbital (LUMO). Electrons can transfer from the dye molecules to the catalyst, leading to the ROS generation for initiating the photodegradation process. This last mechanism takes place when the incident photon energy is not sufficient to excite the photocatalyst, providing that its CB is more positive than the LUMO of the dyes [12]. Whatever the mechanism, it is however necessary that the dye molecules are adsorbed on the catalyst surface. For this reason, it is highly favorable to have nanosized particles, i.e. in the range from 1 to 100 nm, in order to offer a higher surface area compared to micro-particles or bulk materials.

Many studies focused their attention on different semiconductors and their photocatalytic capabilities. In particular, titanium dioxide (TiO_2) has been one of the most extensively investigated materials in this regard, and it has proved to possess excellent photocatalytic properties to degrade a large number of polluting compounds [13–15]. Zinc oxide (ZnO) is another semiconductor that gathered great attention as a possible purifying agent for dye-contaminated wastewater. ZnO also shows a good photocatalytic activity, low cost, and non-toxicity [16–18]. However, both materials are characterized by a wide band gap (3.2 eV for TiO_2 and 3.37 eV for ZnO) which limits their optical absorption capabilities to the ultraviolet (UV) spectrum, thus hindering their photocatalytic applicability [19, 20]. Moreover, such applicability is further affected by the rapid recombination rate of photogenerated electron–hole pairs, which plays a pivotal role in the photocatalytic process. In this respect, many efforts have been made to improve the photodegradation capabilities of semiconductors through different approaches. Doping and structure modification exploiting different materials, such as Au, Ag, Pd, Al, and Mn among others, have been investigated as viable strategies to enhance the efficacy of photocatalysts [21, 22]. The introduction of dopants in their crystal structure has been shown to increase photon absorption, potentially enhancing the performance of photocatalysis [23]. Indeed, the presence of defects states given by the foreign atom in the crystal may potentially reduce the energy required to trigger the excitation of electrons from the valence band to the conduction band. This effect can increase the region of solar light absorbed by the photocatalysts and its consequent feasibility in industrial applications. To further contrast the fast electron–hole pairs recombination and the inadequate degradation efficacy of various photocatalysts, other works focused their attention on the investigation of multicomponent heterojunctions to obtain better performing photocatalytic systems [24, 25]. Finally, other studies focused their attention on the sensitization-mediated photodegradation process. Indeed, increasing the efficiency of dye adsorption on the catalyst surface [26–30] can potentially increase the photodegradation performances, limiting the chances of electron–hole recombination.

In this respect, various strategies can be adopted to physically adsorb the dye at the catalysts surface and thus maintaining it close to the source of photogenerated ROS. In the case of metal oxide nanoparticles, like ZnO, various chemical functionalization using silane, carboxyl, phosphonate, catechol, amine or thiol group, can be adopted to modify the

surface and improve the interaction with the adsorbing dye molecule, depending of the type of compound. Manifold chemical moieties or coating polymers can be used on the ZnO photocatalyst, or other nanoparticles or thin coating inorganic films can be grafted, as reported elsewhere by some of us [31].

In view of the hazardous and harmful behavior of RhB in wastewaters and with the purpose of further improving the photocatalysis phenomenon performances, in the present work ZnO nanoparticles (NPs) were synthesized exploiting a fast and cost-effective wet-chemical method. Aiming to exploit the surface adsorption of the dye, a stabilizing agent, i.e. oleic acid, was used during the wet-chemical synthesis and its role was evaluated in the RhB adsorption process. Furthermore, gadolinium and iron were tested as doping elements to determine whether crystal or band gap modification of the ZnO semiconductor can be a foremost aspect in the performance of the dye photodegradation. The synthesized nanoparticles were extensively characterized in terms of morphology, crystalline structure, surface charge, and hydrodynamic size, and their optical properties have been assessed. UV–Vis measurements were then performed to determine the adsorption and photocatalytic capabilities of the different NPs towards Rhodamine B in solution, also focusing on the possible degradation mechanisms. Particular attention was put on reactive oxygen species generation through Electronic Paramagnetic Resonance (EPR) spectroscopy and fluorescence measurement, seeking for a common thread connecting ROS production to the adsorption and photocatalytic degradation results.

Throughout the whole process, the role of both the doping agents and the oleic acid in the photodegradation efficiency was deeply examined and investigated at the nanosized scale. Different levels of efficiency in the RhB photodegradation up to complete degradation were observed. Particular attention was paid to the introduction of oleic acid as a capping agent on the NPs surface, focusing on its importance in the interaction between the nanoparticles and the dye molecules. The contribution that this parameter brings to the initiation of the whole photocatalytic process was carefully investigated, also in connection with the effects of ROS generation on the degradation mechanism.

2 Materials and methods

2.1 Synthesis of undoped and doped zinc oxide nanoparticles

Undoped and gadolinium- and iron-doped zinc oxide NPs were synthesized through a wet chemical method, exploiting oleic acid as a stabilizing agent [32, 33].

For the synthesis of the undoped zinc oxide NPs, 40 mL of ethanol (99%, Sigma-Aldrich) was put in a 100 round-bottom flask. Then, 526 mg of zinc acetate dihydrate ($Zn(CH_3COO)_2 \cdot 2H_2O$, ACS Reagent, $\geq$ 99.0%, Sigma-Aldrich, Darmstadt, Germany) was dissolved in the flask before adding 1 mL of double distilled water (obtained from a Direct Q3 system, Millipore, Burlington, MA, USA) and 140 μl of oleic acid ($\geq$ 99%, Sigma-Aldrich). The whole system, closed in refluxing conditions with a refrigerating column, was then placed on a stirring plate (VELP Scientifica ARE Hot plate stirrer) at 350 revolutions per minute (rpm) and heated up to 70 °C exploiting a silicon oil bath, which was put in contact with the bottom of the flask. In the meantime, a solution made by 0.522 g of TMAH (Tetramethylammonium hydroxide, 98.5%, Sigma-Aldrich) dissolved in 1.052 mL of double distilled water (obtained by a Direct Q3 system, Millipore) and 10 mL of ethanol was prepared and quickly poured in the flask 10 min after the desired temperature was reached. The reaction was carried out for further 5 min, after which 40 mL of ice-cold (0–4 °C) ethanol was added in the flask, which was then put in an ice bath for 3 min. Finally, the resulting solution was subjected to two washing steps by centrifuging it at 8000 g for 10 min, and the obtained oleate-stabilized, zinc oxide nanoparticles (Ol–ZnO NPs) were stored in fresh ethanol.

The synthesis of oleate-stabilized gadolinium-doped (Ol–ZnO–Gd, 12 at% of doping) and oleate-stabilized iron-doped (Ol–ZnO–Fe, 6 at% of doping) NPs was performed in a similar manner, adding respectively 96.3 mg of Gadolinium(III) acetate hydrate ($Gd(CH_3COO)_3 \cdot H_2O$, from Sigma-Aldrich) and 58 mg of ferric nitrate nonahydrate ($Fe(NO_3)_3 \cdot 9H_2O$, HiMedia) in the round-bottom flask together with the zinc precursor. In both cases, the synthesis was carried out for 10 min after the addition of the TMAH-based solution.

As a control, both the undoped nanoparticles (ZnO NPs) and the doped ones (ZnO–Gd NPs and ZnO–Fe NPs) were synthesized without using the stabilizing agent, i.e. oleic acid, by performing the exact same procedure without the addition of the 140 μL of oleic acid in the process.

2.2 Physicochemical characterization of the oleate-stabilized nanoparticles

Field emission scanning electron microscopy (FESEM, SUPRA 40 from Zeiss, Oberkochen, Germany) analyses were performed to evaluate the morphology and the chemical composition of the synthesized nanoparticles. The samples preparation required the use of a 100 µg/mL concentrated solution of NPs in water, from which 10 µL was spotted and dried on a flat silicon substrate before the measurements.

To assess the crystallinity of the oleate-stabilized NPs, X-ray diffraction measurements were carried out by dispersing 1 mg of nanoparticles in 50 µL of fresh ethanol, letting the prepared sample dry on a silicon wafer substrate, and analyzing it through a Panalytical X'Pert PRO diffractometer in Bragg–Brentano configuration, equipped with a CuKα monochromatic radiation ($\lambda = 1.54059$ Å) as X-ray source.

Dynamic light scattering (DLS) measurements were performed to determine the hydrodynamic radius of the synthesized nanoparticles. To this aim, 100 µg of NPs was dispersed in 1 mL of double distilled water, and the prepared solution was analyzed exploiting Zetasizer Nano ZS90 (Malvern Panalytical, Malvern, UK). The same instrument was used to evaluate how the surface charge of the nanoparticles varies with the pH through Z-potential measurements. The sample preparation was carried out as it did for the DLS analyses, and the pH was adjusted from 2 to 11 with HCl and NaOH 1 M.

Finally, the optical properties of the oleate-stabilized nanocrystals in the ultraviolet and visible region of the light spectrum were investigated in transmission mode through a double-beam Varian Cary 5000 UV–vis-NIR spectrophotometer. Specifically, a 2 mg/mL concentrated solution of NPs in ethanol was prepared and put in a quartz cuvette (350 µL volume, 1 mm optical path length). During the analysis, a pure ethanol sample as a baseline curve was analyzed for background subtraction.

DLS, Z-potential, and UV–Vis analyses were performed also on the control nanocrystals (the one synthesized without oleic acid), and the results are reported in the Supporting Information file (Fig. S2).

2.3 Rhodamine B adsorption and degradation tests

The aim of this study was to investigate the photodegradation of RhB under simulated solar light utilizing the synthesized oleate-stabilized nanoparticles (both doped and undoped) as catalysts during the reaction. To assess the potential role of the oleic acid, and possibly of the different doping agents, within this degradation mechanism, the same nanoparticles synthesized without the stabilizing agent were used as control.

The experiment was carried out exploiting a white lamp (Schölly Fiberoptic GMBH, Flexilux 650, Endoscopy Fiber-Optic Light Source 150W) that emits a radiation composed mainly of visible light (150 W/m^2) and about 4% of UV light (0.17 W/m^2) to simulate solar light. More specifically, a Pyrex type reactor, covered with an aluminum foil, was filled with 10 mL of a 2.5 ppm concentrated dye solution at 5.8 pH. Each time, the different catalysts were dispersed at a concentration of 0.5 mg/mL. The photodegradation of RhB alone, i.e. without any type of nanoparticle present in the solution, was also evaluated as control. The first assessed parameter was the adsorption of the dye on the nanoparticles surface. To this aim, the reactor was put on a stirring plate at 350 rpm and left in complete dark for 60 min, the time necessary to secure the establishment of an adsorption/desorption equilibrium of the dye on the surface of the catalyst. After this time, 300 µL of the solution was collected, centrifuged at 14000 g for 10 min and two replicates of 100 µL of the supernatant were analyzed with a UV–Vis spectrophotometer (Multiskan FC, Thermo Scientific), coupled with the Thermo Scientific SkanIt Software for data collection. Considering the corresponding absorbance value, the adsorption values were calculated for each catalyst through the following equation:

$$\text{Adsorption}\,(\%) = \left(1 - \frac{C_{RhB60}}{C_{RhB0}}\right) * 100$$

where C_{RhB60} is the dye concentration at the end of the adsorption phase and C_{RhB0} represents the initial Rhodamine B concentration. The maximum amount of dye adsorbed on the NPs surface (q_{max}) was also calculated.

Once the adsorption of the dye on the different catalysts was evaluated, the photodegradation test was performed. The solution in the reactor was left under stirring conditions, the lamp was switched on, and the RhB degradation was measured at 2, 4, 6, 8, 10, 20, and 30 min. After each time step (starting from time 0, corresponding to the end of the 60 min of the adsorption phase), 200 µL of the solution was collected and directly analyzed in two replicates with the UV–Vis spectrophotometer. Since no centrifugation step was provided in this case, a different calibration curve for each

catalyst in the dye solution was used to determine the concentration of RhB after each time step (Supporting Information file, Fig. S1). The dye degradation was measured as C/C_0, where C is the concentration of RhB in the solution in which the catalyst was dispersed at the considered time step, and C_0 is the dye concentration in the same solution at time 0. Such concentrations were measured each time considering the absorbance value at the wavelength corresponding to the absorbance peak of Rhodamine B.

2.4 Analysis of the degradation mechanism

To better understand the mechanism underlying the dye degradation in presence of the different catalysts, the characteristic RhB absorbance peak was analyzed throughout the photocatalysis process. The photodegradation experiment was repeated with the same setup and parameters for all the types of nanoparticles, and after 2 and 30 min 100 µL of the solution was collected and directly analyzed with the UV–Vis spectrophotometer, where the absorbance spectrum between 450 and 700 nm was recorded. This procedure allowed to investigate if a peak shift occurred together with the corresponding lowering of its absorbance value.

2.5 Analysis of reactive oxygen species generation

Reactive oxygen species seem to play an important role in RhB degradation [34–36]. To better understand if some of these species are generated during the dye photodegradation process, two different experiments were carried out. The first one was aimed at the detection of the generated hydroxyl radicals ·OH through Electron Paramagnetic Resonance (EPR) spectroscopy, exploiting an EMXNanoX-Band spectrometer (Bruker) assisted by the spin-trap molecule 5,5-dimethyl-1-pyrroline-N-Oxide (DMPO, Sigma-Aldrich). For these measurements, 1.8 mL of RhB solution, in which the catalyst was dispersed, was mixed with 200 µL of a solution of DMPO in double distilled water. The final 2 mL solution, whose concentrations were 2.5 ppm for the dye, 0.5 mg/mL for the catalyst, and 10 mM for the spin-trap molecule, was put in a 24-well plate, which was left in the dark for 60 min (to establish the adsorption/desorption equilibrium) before being subjected to the same radiation conditions used for the photodegradation experiment. After 10 min, 50 µL of the solution was transferred in a quartz capillary tube and analyzed to investigate the production of the DMPO-OH adduct.

For the second experiment a detection reagent, namely Singlet Oxygen Sensor Green (SOSG, TermoFisher), was exploited to examine the generation of singlet oxygen ($^1O_2$). To this aim, 2 µL of SOSG dissolved in methanol was added to 2 mL of the 2.5 ppm concentrated dye solution in which the catalyst was dispersed at 0.5 mg/mL concentration, in order to reach a final molar concentration of the detection reagent equal to 5 µM. The solution was put in a well of a 24-well plate, left in the dark for 60 min and then irradiated at the same radiation conditions as before. At the end of the dark phase (before the irradiation procedure), 100 µL of the solution was collected, put in a 96-well plate and analyzed through a fluorescence signal measurement with a SynergyTM HTX Multi-Mode Microplate Reader (BioTek). The same procedure was repeated after 10 min of irradiation.

Both the abovementioned experiments were performed with all different types of nanoparticles redispersed both in RhB solution at 2.5 ppm and in double distilled water, to investigate if the presence of the dye in the solution influences the possible ROS generation. Control measurements in absence of the catalysts were also performed.

3 Results and discussion

3.1 Physicochemical characterization of the oleate-stabilized nanoparticles

The synthesis of oleic acid capped ZnO NPs with Iron or Gadiolinum as doping agents was performed with awet-chemical method and comparative synthesis were performed without capping agent or without doping. After their synthesis, a complete physicochemical characterization was performed on the nanoparticles.

FESEM measurements (Fig. 1a) on Ol–ZnO, OI–ZnO–Gd, Ol–ZnO–Fe NPs show round-shaped nanoparticles in all three samples, with a diameter of around 6–10 nm. The absence of differences in size and morphology between the undoped and the doped nanoparticles may be attributed to the dominance of the steric effects of the reagents
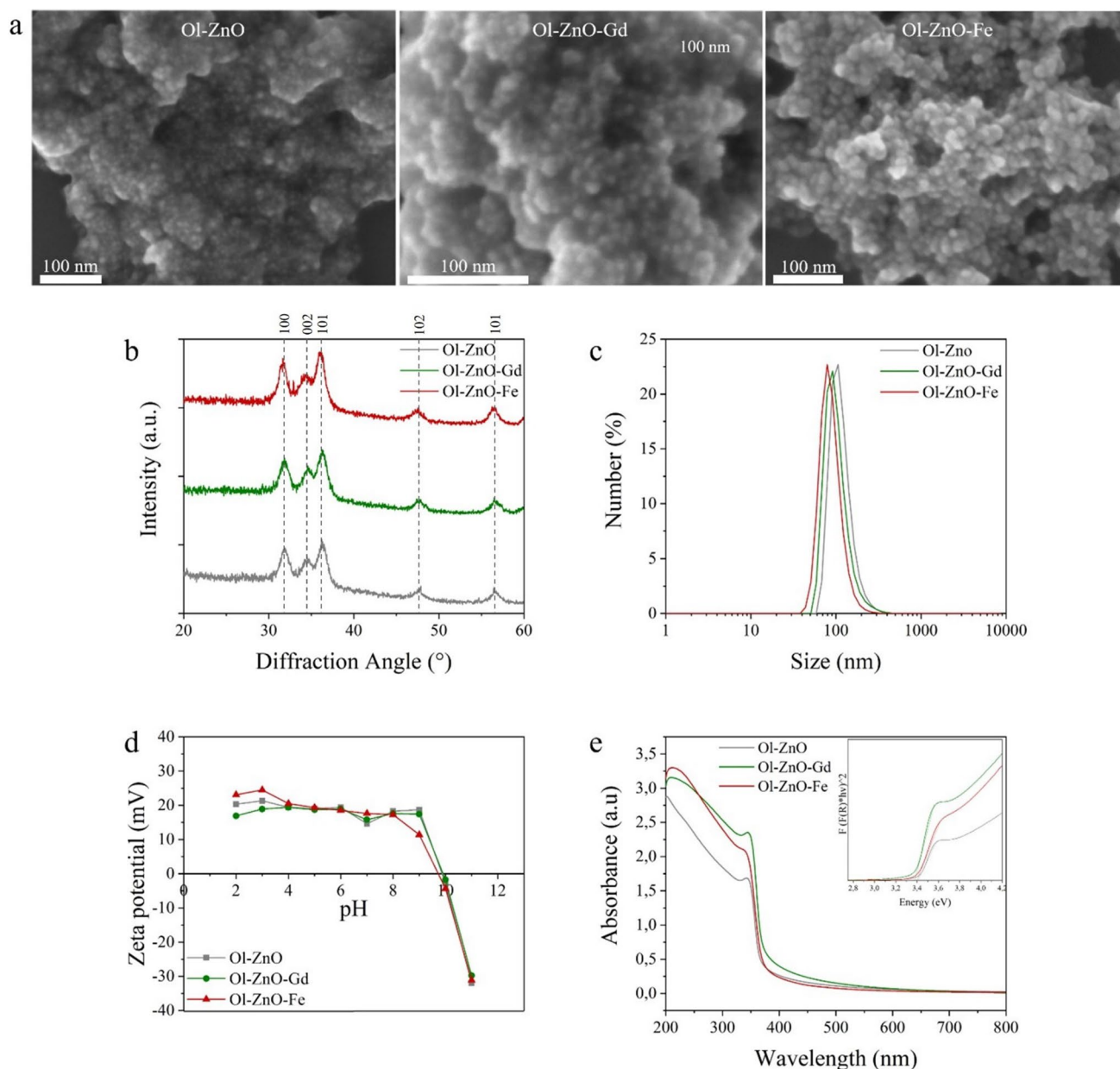
Fig. 1 Characterization of the oleate-stabilized, undoped and doped zinc oxide nanoparticles: **a** Field emission scanning electron microscopy (FESEM) images; **b** X-ray diffraction pattern of the synthesized NPs; **c** Size distribution resulting from Dynamic Light Scattering (DLS) measurements in double distilled water; **d** Trend of the Z-potential values of the analyzed nanoparticles varying the pH of the solution between 2 and 11; **e** UV–visible spectra with the Tauc's plots for the evaluation of the optical band gaps (Eg) represented in the upper right square

exploited in the synthesis procedure, which contrast the tendency, reported in the literature [37], of a decrease of the particles size upon doping.

The crystallinity of the oleate-stabilized nanoparticles was investigated through X-ray diffraction, and the results are reported in Fig. 1b. The spectra resulting from these analyses highlight the presence of the characteristic diffraction peaks of the ZnO wurtzitic structure (JCPDS-ICDD (card No. 89-1397)). Furthermore, it confirms the successful doping procedure of the ZnO structure since no additional peaks related to the formation of new crystalline phases are observable. Also, XPS analyses performed on similarly obtained NPs in other works [32, 33] indicate the presence of the doping element for Ol–ZnO–Gd and Ol–ZnO–Fe, with the presence of both the iron oxidation states (Fe^{2+} and Fe^{3+}) in the iron-doped ZnO NPs.

Table 1 Adsorption values in % and in mass (q$_{max}$ expressed in mg per g of NPs) of Rhodamine B on the different nanoparticles surface

Catalyst	RhB adsorption (%)	q$_{max}$ (mg/g of NPs)
Ol–ZnO	80.9	4.05
Ol–ZnO–Gd	83.6	4.18
Ol–ZnO–Fe	82.6	4.13
ZnO	46.5	2.33
ZnO–Gd	46.1	2.31
ZnO–Fe	43.1	2.16

DLS measurements were performed to evaluate the hydrodynamic diameter and the colloidal stability of the nanoparticles in double distilled water (Fig. 1c). The graph exhibits a narrow size distribution for all the three samples analyzed, with peaks at 106, 91.3, and 78.8 nm and polydispersity indexes (PDI) of 0.094, 0.143, and 0.161 for Ol–ZnO, Ol–ZnO–Gd, and Ol–ZnO–Fe NPs, respectively. The discrepancy between the values of the hydrodynamic diameters and the ones derived from FESEM analyses may be explained by the fact that DLS measurements are performed on NPs suspended in water, thus their steric hindrance, as well as adsorption of ions on their surface, should be considered. However, the possibility of the formation of small aggregates cannot be excluded. Similar results were obtained for the uncapped ZnO NPs, as reported in Figure S2a of the Supporting Information.

In this respect, we observed that all the NPs synthesized via this wet-chemical synthesis with or without oleic acid have comparable characteristics and sizes. In particular, no aggregation is evidenced for ZnO NPs synthesized without capping agents. We can assume that the surface properties of the samples synthesized in our work are optimal in the used reaction condition, avoiding heavy aggregation of the nanoparticles. However, the use of oleic acid in chemical synthesis is highly beneficial and preferrable as it stabilizes the NPs against aggregation, even for long time periods, and greatly improves the RhB adsorption, as reported below.

Since it has been reported in the literature that RhB photocatalytic degradation proceeds on the catalyst surface rather than in the bulk solution [38], the surface charge of the synthesized nanoparticles is an important parameter to take into consideration, given that it could also influence the adsorption of molecules on the catalyst surface [39, 40]. Therefore, Z-potential measurements were performed on the oleate-stabilized nanoparticles, and the surface charge was monitored at different pH values. The results (Fig. 1d) highlight positive surface charge values for all the samples up until a pH of around 10, where the Z-potential starts to become negative before reaching highly negative values (~ − 30 mV) at pH 11. At the pH conditions of the photodegradation experiment (pH = 5.8), the analyzed nanoparticles thus exhibit a positive surface charge value of around + 20 mV for all the samples, which also explains the high monodisperse degree gathered from the DLS measurements. Similar data were also recorded for the uncapped NPS, as reported in Figure S2b.

Finally, the optical properties of the oleate-stabilized NPs were analyzed, since their analysis could be of great importance in better understanding the photocatalytic degradation process. To this aim, the absorption spectra of Ol–ZnO, Ol–ZnO–Gd, and Ol–ZnO–Fe NPs were recorded, and the results are shown in Fig. 1e. All the samples display a strong absorption in the ultraviolet region, with the Ol–ZnO–Fe nanoparticles that present a modest absorption increase in the visible region, which is slightly more evident for the Gd-doped NPs. The Tauc's plot was exploited to calculate the optical band gaps through the direct semi-conductor equation, and the resulting values are 3.41, 3.38, and 3.39 eV for Ol–ZnO, Ol–ZnO–Gd, and Ol–ZnO–Fe NPs respectively. The absorption spectra were also recorded for the uncapped NPs (Fig. S2c), and the resulting band gap values are 3.29, 3.27, and 3.33 eV for ZnO, ZnO–Gd, and ZnO–Fe NPs respectively.

3.2 RhB adsorption and photodegradation

Before investigating the photocatalytic process of Rhodamine B, its adsorption on the catalysts surface at the end of the dark phase was evaluated to possibly gather more insights about the photodegradation efficiency obtained in the next experiments. The adsorption percentage and q$_{max}$ values are reported in Table 1.

While there is no appreciable discrepancy of the adsorption values between the undoped and the doped nanoparticles, a marked adsorption increase is observable for the NPs synthesized exploiting the capping agent. The aliphatic chain of oleic acid can indeed easily interact with the organic and aromatic groups present in the Rhodamne B molecules, allowing an easier accommodation of such molecules on the Ol–ZnO NPs surface than on the ZnO NPs one without oleic

Fig. 2 RhB degradation trends vs time obtained by photocatalysis with the different types of NPs; the degradation of RhB alone without any catalyst in solution is also reported
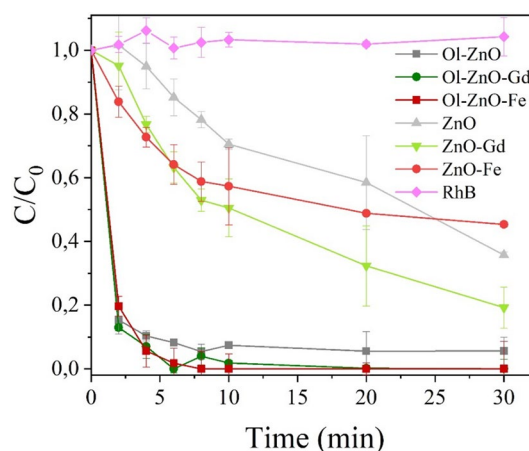
acid. These results seem to suggest that oleic acid plays a pivotal role in the dye adsorption mechanism on the catalysts surface, which may lead to different photocatalytic performances.

Once the adsorption rate was assessed on the catalysts surface, the photodegradation experiments were carried out as reported in Sect. 2.3.

The results, shown in Fig. 2, raise several different discussion points and observations. First of all, it is clear that the presence of whatever type of nanoparticle is necessary to obtain the dye degradation: in fact, no RhB photodegradation is noticeable under the applied experimental conditions in absence of a catalyst in the solution.

The clearest feature inferable from the graph analysis is the extremely significant improvement in RhB photodegradation performances of the oleic-acid capped nanoparticles. In particular, an effective dye degradation is reached already within the first 2 min of the reaction, with RhB degradation values of 85%, 87%, and 81% for Ol–ZnO, Ol–ZnO–Gd, and Ol–ZnO–Fe, respectively, compared to values of 0%, 5%, and 17% for their counterparties synthesized without the stabilizing agent. After 30 min of solution photoirradiation, the complete dye degradation was obtained exploiting Ol–ZnO–Gd and Ol–ZnO–Fe nanoparticles, and a 95% degradation with the undoped Ol–ZnO ones. In contrast, the use of ZnO, ZnO–Gd, and ZnO–Fe NPs as photocatalyst leads to a photodegradation of 65%, 80%, and 55%, respectively, at the end of the reaction.

Concerning the NPs doping, slight improvements in the photocatalysis performances are visible when Gd and Fe atoms are added to the ZnO lattice. This is more evident in the first 10 min in the case of the NPs synthesized without oleic acid. Differently, for the oleate-stabilized NPs, the use of doping elements has a minor difference on the photodegradation efficiency, appreciable at the end of the experiment. The band gap values of the NPs synthesized with and without oleic acid allow to make some further considerations: firstly, the values obtained for the uncapped nanoparticles are in accordance with the results of the photodegradation tests, in which ZnO–Gd NPs were the most efficient, followed by ZnO and ZnO–Fe NPs. These discrepancies are however minimal and the role of the band gap fades into the background when compared to the role of oleic acid. In fact, the oleate-stabilized NPs were extremely more efficient in RhB degradation with respect to their doping and band gap value. This behavior confirms the oleic acid role in the dye adsorption at the nanoparticles surface and in turn its main effect in the overall photodegradation process.

These results, together with the ones obtained in the adsorption tests, seem to suggest that the dye adsorption on the catalysts surface is of great importance for its photodegradation, with oleic acid, more than the doping agent, playing a pivotal role in it.

3.3 Analysis of the degradation mechanism

To better understand the mechanism underlying the photodegradation process, the variation of the absorption spectra was analyzed after 2 and 30 min of irradiation for all samples (Fig. 3).

It has been reported in the literature [38–40] that two different behaviors of the absorbance peak can take place, related to two different mechanisms of RhB degradation. The first one involves a blue-shift of the peak (hypsochromic shift) and it is related to N-deethylation of the dye with the formation of a series of N-deethylated intermediates, while the second one, more strictly related to the color decay of the solution, consists in a decrease of intensity of the absorbance
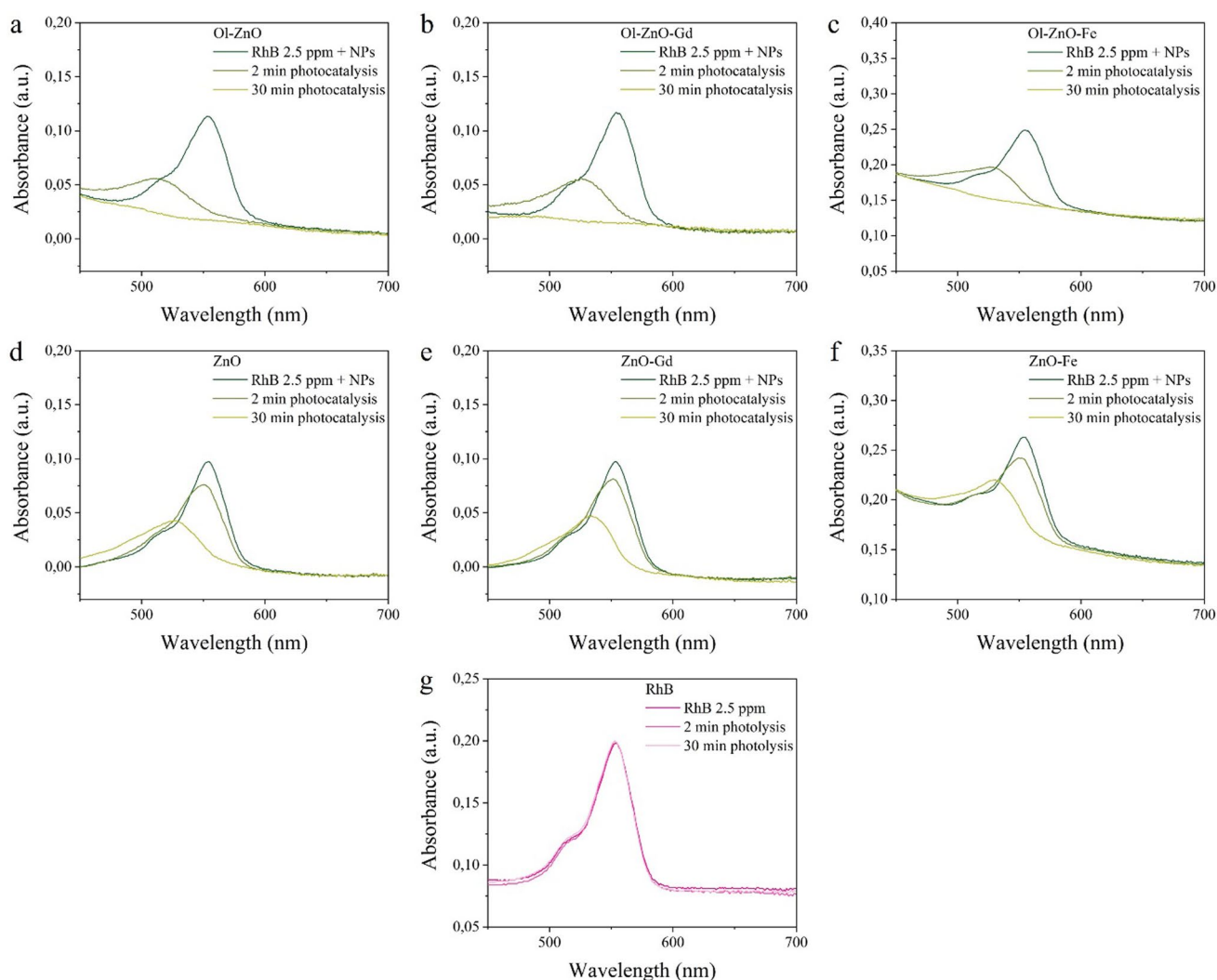
Fig. 3 UV–Vis spectra variation after 2 and 30 min of irradiation of RhB solution using **a** Ol–ZnO, **b** Ol–ZnO–Gd, **c** Ol–ZnO–Fe, **d** ZnO, **e** ZnO–Gd, and **f** ZnO–Fe nanoparticles as catalysts. **g** The spectrum of RhB alone was also collected

peak without any shift in wavelength. This last phenomenon is indicative of the cleavage of the xhantene group, which is the chromophore group.

On that basis, the absorbance spectra in Fig. 3 suggest that for both oleate-stabilized and uncapped NPs the two underlined mechanisms take place simultaneously. In particular, a marked blue-shift of the absorbance peak, complemented by a significant intensity reduction, is already noticeable after 2 min in the case of the oleate-stabilized NPs, with the peak completely disappearing after 30 min as a sign of a complete dye degradation (Fig. 3a, b and c). This whole process is way slower and smoother when ZnO, ZnO–Gd, and ZnO–Fe nanoparticles are exploited as catalysts (Fig. 3d, e and f).

The collective behavior of the different catalysts in relation to the two different mechanisms of RhB degradation are compared: Fig. 4a highlights the values of UV–Vis peak shift for all types of nanoparticles after 2 min of irradiation, claiming for the high hypsochromic shift and thus of the N-deethylation of the dye when using oleate-stabilized NPs. Figure 4b illustrates the great difference of the RhB solution color decay at the end of the 30 min irradiation, exploiting Ol-ZnO (upper panel) and ZnO (lower panel) NPs as catalysts. This phenomenon also highlights the important splitting of the chromophore group, as a result of the cleavage of the xhantene group of RhB, mainly operated by the oleate-stabilized NPs.

Fig. 4 a Analysis of the blue-shift of the absorbance peak after 2 min of irradiation with all the different catalysts in solution, and **b** example of the effect of the combination of simulated solar light irradiation (for 30 min) and Ol–ZnO (upper panel) and ZnO (lower panel) catalysts on the color decay of RhB solution
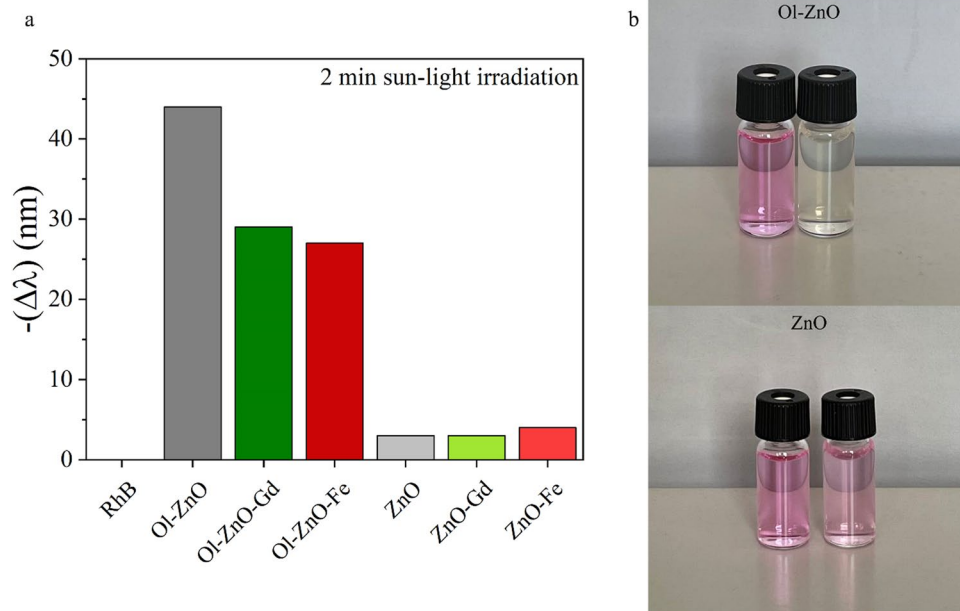

3.4 Analysis of reactive oxygen species generation

Since ROS are demonstrated to play an important role in RhB degradation, their generation was investigated through EPR (in the case of hydroxyl radicals ·OH, in Fig. 5) and fluorescence (in the case of singlet oxygen) measurements, Fig. 6.

The graph derived from the ·OH generation analysis in Fig. 5 exemplary shows the spectra related to the Ol–ZnO and ZnO samples, as well as the RhB solution without any catalyst, all compared to a reference DMPO-OH adduct spectrum. It is worth noting that all EPR measurements carried out for all the analyzed catalysts, both in RhB solution and in double distilled water, resulted in flat spectra as the ones examined and representatively depicted in the graph. This implies that no ·OH radicals were generated during the photocatalysis process, and that the dye degradation was not due to the action of this type of reactive oxygen species. In the case of ZnO nanoparticles, slight peaks attributable to the DMPO-OH adduct are noticeable, but their negligible intensity does not justify the comparably higher degree of RhB degradation.

Concerning the investigation of $^1O_2$ generation, the results are shown in Fig. 6: the fluorescence signals are reported for all the analyzed samples both in RhB solution and double distilled water. They were recorded both after the dark phase and after 10 min of light irradiation and referred to the control, namely the signal derived from RhB solution after the 60 min of dark phase.

Fig. 5 EPR spectra obtained exploiting the DMPO spin trap after 10 min of light irradiation
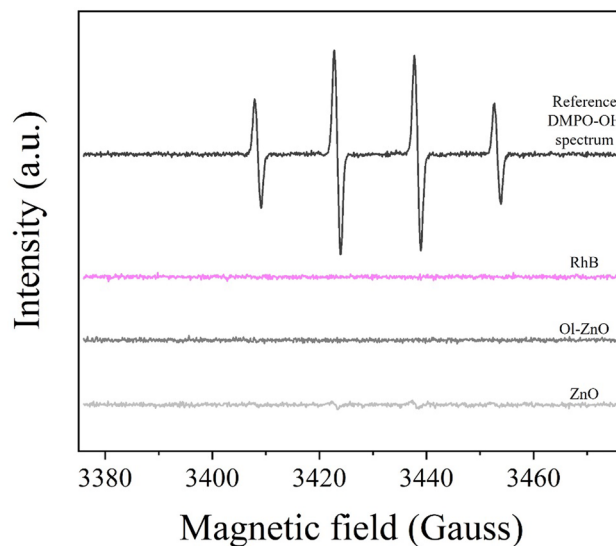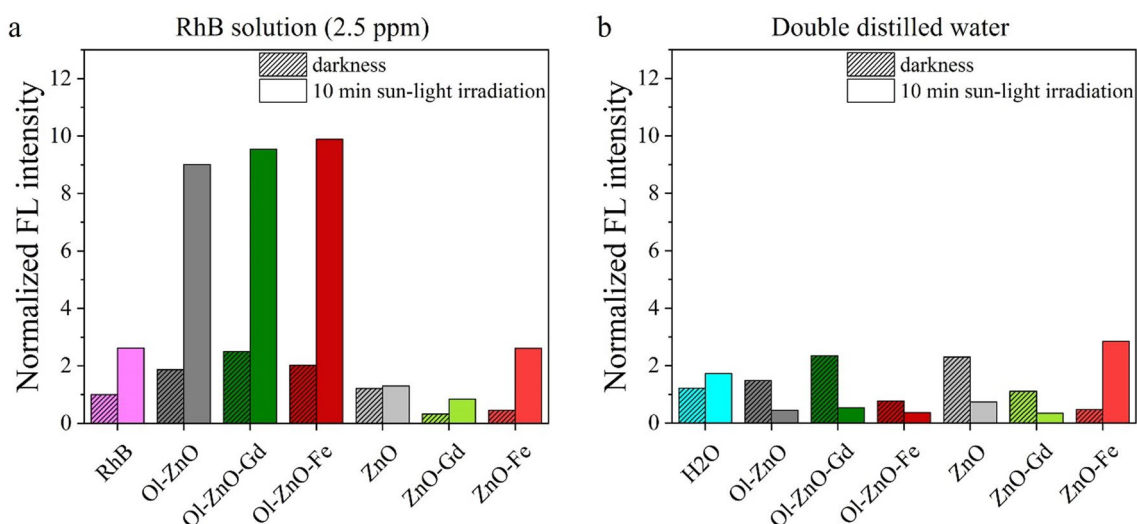
Fig. 6 Fluorescence signal analysis related to singlet oxygen generation exploiting SOSG detection reagent

These results highlight a significant difference in singlet oxygen generation between the oleate-stabilized catalysts and the ones synthesized without oleic acid. Furthermore, this radical production is limited to the irradiation phase and only occurs in presence of RhB in solution (Fig. 6a). The fact that no $^1O_2$ generation is detected in double distilled water (Fig. 6b) indicates that RhB presence in the solution is crucial for its production, as well as the presence of catalysts in the solution, specifically the oleate-stabilized ones. It is worth mentioning that for the catalysts synthesized without the stabilizing agent, the measured fluorescence values and their inter-sample discrepancy is limited within the noise measurements, being these values equal or slightly below the one obtained irradiating the RhB solution alone. Considering these results and the ones derived from the adsorption tests, it becomes clear that the significantly higher singlet oxygen generation detected for Ol–ZnO, Ol–ZnO–Gd, and Ol–ZnO–Fe NPs is strictly related to the considerably greater adsorption rate measured for these catalysts compared to the one calculated for the NPs without oleic acid. The high adsorption rate of RhB on the oleate-stabilized catalysts surface triggers singlet oxygen production upon light irradiation, which leads to a great photodegradation efficiency, in line with the degradation tests results.

Taken together, all these considerations shed light on the dye degradation process. In particular, the adsorption, degradation, and ROS generation tests suggest that RhB degradation occurs through the dye-sensitization phenomenon, in which a dye (Rhodamine B in this case), adsorbed on a nanosized catalyst surface, can be excited at the wavelengths of light in the solar spectrum, leading to the electron transfer from the highest occupied molecular orbital (HOMO) to the LUMO of the photocatalyst, thus triggering its own degradation pathway [12, 41].

For the catalysts analyzed in this work, $^1O_2$ seems the main responsible for RhB degradation, at least in the case of the oleate-stabilized nanoparticles. No singlet oxygen production is in contrast detected in the case of the NPs synthesized without oleic acid. However, it should be mentioned that these measurements are related to a 10 min irradiation, which is the most relevant time in the present work. Furthermore, this is a time after which the dye degradation rate exploiting ZnO, ZnO–Gd, and ZnO–Fe NPs is minimal. Thus, the generation of reactive oxygen species could still be an important factor in RhB degradation at longer light exposures.

4 Conclusions

In the present paper, we have proposed the use of nanosized photocatalysts made of zinc oxide nanoparticles to degrade a polluting dye under simulated solar radiation. To enhance the mechanism of RhB degradation, here used as a representative pollutant of industrial wastewater, we exploited the role of doping and surface functionalization. Spherical ZnO NPs were fabricated with different doping elements (gadolinium and iron) and their photocatalytic performance compared their undoped counterparts. A rapid dye adsorption on the photocatalyst surface was obtained by surface modification through oleic acid, with outstanding increase in terms of dye degradation. Indeed, an efficient generation

of ROS, in particular singlet oxygen, was detected and an ultra-rapid degradation of the RhB dye was then achieved within 10 min of simulated solar light irradiation conditions. ZnO NPs were shown to be very efficient photocatalysts in all the analysed forms, still the surface modification plays a major role in the degradation of the dye almost doubling the performance of uncapped ZnO NPs. Interestingly, the doping induces only very slight enhancements in the photo-degradation process, indicating that the surface properties are of foremost importance in the overall characteristics of the photocatalyst. This work thus proposes an extremely promising tool for wastewater remediation and shows how the fine control of surface properties and nanosized structures can greatly enhance the photocatalytic efficiency up to the complete degradation of organic pollutants.

Author contribution N.M. Percivalle conducted the experimental work, wrote the main manuscipt, prepared Figs. 1, 2, 3, 4, 5, 6; M.C. assisted in the experiments and developed the methodology; M.C., S.H. and V.C. supervsed the work, ideated the study and revised the main manuscript.

Data availability Data is provided within the manuscript or supplementary information files.

Declarations

Competing interests The authors declare no competing interests.

References

1. Mazhar MA, et al. Chlorination disinfection by-products in municipal drinking water—a review. J Clean Prod. 2020;273:123159. https://doi.org/10.1016/j.jclepro.2020.123159.
2. Sulaiman AA, Attalla FE, Sherif MAS, Keshk K. Water pollution: source & treatment. Water Pollut Source Treat. 2016;6(3):88–98. https://doi.org/10.5923/j.ajee.20160603.02.
3. Fn C, Mf M. Factors affecting water pollution: a review. J Ecosyst Ecography. 2017. https://doi.org/10.4172/2157-7625.1000225.
4. Lellis B, Fávaro-Polonio CZ, Pamphile JA, Polonio JC. Effects of textile dyes on health and the environment and bioremediation potential of living organisms. Biotechnol Res Innov. 2019. https://doi.org/10.1016/j.biori.2019.09.001.
5. Rafiq A, et al. Photocatalytic degradation of dyes using semiconductor photocatalysts to clean industrial water pollution. J Ind Eng Chem. 2021;97:111–28. https://doi.org/10.1016/j.jiec.2021.02.017.
6. Merouani S, Hamdaoui O, Saoudi F, Chiha M. Sonochemical degradation of Rhodamine B in aqueous phase: effects of additives. Chem Eng J. 2010;158:550–7. https://doi.org/10.1016/j.cej.2010.01.048.
7. Hartley TW. Public perception and participation in water reuse». Desalination. 2006;187:115–26. https://doi.org/10.1016/j.desal.2005.04.072.
8. Ong CB, Ng LY, Mohammad AW. A review of ZnO nanoparticles as solar photocatalysts: synthesis, mechanisms and applications. Renew Sustain Energy Rev. 2018;81:536–51. https://doi.org/10.1016/j.rser.2017.08.020.
9. Krystynik P. Advanced oxidation processes (AOPs)—utilization of hydroxyl radical and singlet oxygen. In: Ahmad R, editor. Biochemistry. London: IntechOpen; 2022. https://doi.org/10.5772/intechopen.98189.
10. Zhang DE, et al. Synthesis and photocatalytic property of multilayered Co_3O_4. Appl Surf Sci. 2015;355:547–52. https://doi.org/10.1016/j.apsusc.2015.04.018.
11. Yuan X, Yang B, Hu X, Dong X, Wei Y, Zhu J. Room-temperature synthesis and solar photocatalytic performance of MoO3·0.5H2O nanorods. Appl Surf Sci. 2015;357:968–74. https://doi.org/10.1016/j.apsusc.2015.08.071.
12. Chiu Y-H, Chang T-F, Chen C-Y, Sone M, Hsu Y-J. Mechanistic insights into photodegradation of organic dyes using heterostructure photocatalysts. Catalysts. 2019;9:430. https://doi.org/10.3390/catal9050430.
13. Fox MA, Dulay MT. Heterogeneous photocatalysis. Chem Rev. 1993;93:341–57. https://doi.org/10.1021/cr00017a016.
14. Kusvuran E, Samil A, Atanur OM, Erbatur O. Photocatalytic degradation kinetics of di- and tri-substituted phenolic compounds in aqueous solution by TiO_2/UV. Appl Catal B Environ. 2005;58:211–6. https://doi.org/10.1016/j.apcatb.2004.11.023.
15. Alaton IA, Balcioglu IA. Photochemical and heterogeneous photocatalytic degradation of waste vinylsulphone dyes: a case study with hydrolyzed Reactive Black 5. J Photochem Photobiol Chem. 2001;141:247–54. https://doi.org/10.1016/S1010-6030(01)00440-3.
16. Lee KM, Lai CW, Ngai KS, Juan JC. Recent developments of zinc oxide based photocatalyst in water treatment technology: a review. Water Res. 2016;88:428–48. https://doi.org/10.1016/j.watres.2015.09.045.

17. Chen X, Wu Z, Liu D, Gao Z. Preparation of ZnO photocatalyst for the efficient and rapid photocatalytic degradation of Azo dyes. Nanoscale Res Lett. 2017;12:143. https://doi.org/10.1186/s11671-017-1904-4.

18. Mohammad A, Kapoor K, Mobin SM. Improved photocatalytic degradation of organic dyes by ZnO-nanoflowers. ChemistrySelect. 2016;1:3483–90. https://doi.org/10.1002/slct.201600476.

19. Miyauchi M, Nakajima A, Watanabe T, Hashimoto K. Photocatalysis and photoinduced hydrophilicity of various metal oxide thin films. Chem Mater. 2002;14:2812–6. https://doi.org/10.1021/cm020076p.

20. Kamarulzaman N, Kasim MF, Rusdi R. Band gap narrowing and widening of ZnO nanostructures and doped materials. Nanoscale Res Lett. 2015;10:346. https://doi.org/10.1186/s11671-015-1034-9.

21. Dhull P, et al. An overview on $InVO_4$-based photocatalysts: electronic properties, synthesis, enhancement strategies, and photocatalytic applications. Mol Catal. 2023;539:113013. https://doi.org/10.1016/j.mcat.2023.113013.

22. Soni V, et al. Current perspective in metal oxide based photocatalysts for virus disinfection: a review. J Environ Manage. 2022;308:114617. https://doi.org/10.1016/j.jenvman.2022.114617.

23. Dutta V, et al. Prism-like integrated Bi_2WO_6 with $Ag-CuBi_2O_4$ on carbon nanotubes (CNTs) as an efficient and robust S-scheme interfacial charge transfer photocatalyst for the removal of organic pollutants from wastewater. Environ Sci Pollut Res. 2022;30:124530–45. https://doi.org/10.1007/s11356-022-20743-8.

24. Kumar A, et al. Rationally constructed synergy between dual-vacancies and Z-scheme heterostructured MoS_2-x/g-C_3N_4/Ca-α-Fe_2O_3 for high-performance photodegradation of sulfamethoxazole antibiotic from aqueous solution. Chem Eng J. 2023;474:145720. https://doi.org/10.1016/j.cej.2023.145720.

25. Malhotra M, et al. An overview of improving photocatalytic activity of MnO_2 via the Z-scheme approach for environmental and energy applications. J Taiwan Inst Chem Eng. 2024;158:104945. https://doi.org/10.1016/j.jtice.2023.104945.

26. Zhang X, et al. Effects of Ag loading on structural and photocatalytic properties of flower-like ZnO microspheres. Appl Surf Sci. 2017;391:476–83. https://doi.org/10.1016/j.apsusc.2016.06.109.

27. Silva CG, et al. Developing highly active photocatalysts: gold-loaded ZnO for solar phenol oxidation. J Catal. 2014;316:182–90. https://doi.org/10.1016/j.jcat.2014.05.010.

28. Zhong JB, et al. Improved photocatalytic performance of Pd-doped ZnO. Curr Appl Phys. 2012;12:998–1001. https://doi.org/10.1016/j.cap.2012.01.003.

29. Rekha K, Nirmala M, Nair MG, Anukaliani A. Structural, optical, photocatalytic and antibacterial activity of zinc oxide and manganese doped zinc oxide nanoparticles. Phys B Condens Matter. 2010;405:3180–5. https://doi.org/10.1016/j.physb.2010.04.042.

30. Islam Molla A, Tateishi I, Furukawa M, Katsumata H, Suzuki T, Kaneco S. Evaluation of reaction mechanism for photocatalytic degradation of dye with self-sensitized TiO_2 under visible light irradiation». Open J Inorg Non-Met Mater. 2017;07:1–7. https://doi.org/10.4236/ojinm.2017.71001.

31. Laurenti M, Stassi S, Canavese G, Cauda V. Surface engineering of nanostructured ZnO surfaces. Adv Mater Interfaces. 2017;4:1600758. https://doi.org/10.1002/admi.201600758.

32. Barui S, Gerbaldo R, Garino N, Brescia R, Laviano F, Cauda V. Facile chemical synthesis of doped ZnO nanocrystals exploiting oleic acid. Nanomaterials. 2020;10:1150. https://doi.org/10.3390/nano10061150.

33. Carofiglio M, et al. Iron-doped ZnO nanoparticles as multifunctional nanoplatforms for theranostics. Nanomaterials. 2021;11:2628. https://doi.org/10.3390/nano11102628.

34. He W, et al. Production of reactive oxygen species and electrons from photoexcited ZnO and ZnS nanoparticles: a comparative study for unraveling their distinct photocatalytic activities. J Phys Chem C. 2016;120:3187–95. https://doi.org/10.1021/acs.jpcc.5b11456.

35. Hu Y, Li D, Wang H, Zeng G, Li X, Shao Y. Role of active oxygen species in the liquid-phase photocatalytic degradation of RhB using $BiVO_4$/TiO_2 heterostructure under visible light irradiation. J Mol Catal Chem. 2015;408:172–8. https://doi.org/10.1016/j.molcata.2015.07.025.

36. Guo A, et al. Singlet oxygen mediated efficient photocatalytic degradation of rhodamine B and disinfection by ZnO@PDA/Ag-Ag_2O nanocomposite under LED light. J Alloys Compd. 2022;928:167138. https://doi.org/10.1016/j.jallcom.2022.167138.

37. Xia T, et al. Decreased dissolution of ZnO by iron doping yields nanoparticles with reduced toxicity in the rodent lung and zebrafish embryos. ACS Nano. 2011;5:1223–35. https://doi.org/10.1021/nn1028482.

38. Chen F, Zhao J, Hidaka H. Highly selective deethylation of rhodamine B: adsorption and photooxidation pathways of the dye on the TiO_2/SiO_2 composite photocatalyst. Int J Photoenergy. 2003;5:209–17. https://doi.org/10.1155/S1110662X03000345.

39. He Z, Sun C, Yang S, Ding Y, He H, Wang Z. Photocatalytic degradation of rhodamine B by Bi2WO6 with electron accepting agent under microwave irradiation: mechanism and pathway. J Hazard Mater. 2009;162:1477–86. https://doi.org/10.1016/j.jhazmat.2008.06.047.

40. Lops C, et al. Sonophotocatalytic degradation mechanisms of Rhodamine B dye via radicals generation by micro- and nano-particles of ZnO. Appl Catal B Environ. 2019;243:629–40. https://doi.org/10.1016/j.apcatb.2018.10.078.

41. Zhou Y, et al. Dye promoted electron transfer in DUT-5/$BiVO_4$ heterojunction for organic pollutants degradation. Mater Res Bull. 2022;150:111740. https://doi.org/10.1016/j.materresbull.2022.111740.

Discover